Supplementary Information for

Reduced N_2 fixation in the Atlantic Ocean during the Warm Late Pliocene

Maayan Yehudai[1]*, Jesse R. Farmer[2], Marietta Straub[3], Anja S. Studer[4], Lukas Oesch[1], Roger C. Creel[5], Ralf Schiebel[1], Alexandra Auderset[6], Kira Lawrence[7], Nazik Ogretmen[8], Gerald H. Haug[1], Daniel M. Sigman[9] and Alfredo Martínez-García[1]*

Maayan Yehudai
Email: m.yehudai@mpic.de

This PDF file includes:

Supplementary text S1 to S4
Supplementary Figures S1 to S9
SI References

Other supporting materials for this manuscript include the following:

Supplementary Data S1 to S3

Supplementary Information Text

S1. Calculation of thermocline - FB-$\delta^{15}N$ from ODP Site 662

Previous work on foraminifera-bound nitrogen isotopes [1,2] indicates that FB-$\delta^{15}N$ of *Trilobatus sacculifer (Tsacc)* is 1-1.5‰ lower than that of the non-symbiotic thermocline dwelling species FB-$\delta^{15}N$ *Neogloboquadrina dutertrei (Ndut)*. This offset between the symbiotic species *Tsacc* and the non-symbiotic species *Ndut* is most likely caused by the uptake of excreted low-$\delta^{15}N$ ammonia by the symbionts and the subsequent internal N cycle to the host, which would lower the $\delta^{15}N$ of the foraminifera organic N. FB-$\delta^{15}N_{Tsacc}$ is thought to be very close to the $\delta^{15}N$ of its food source and thus reflects the $\delta^{15}N$ of supplied nitrate [1]. In contrast, modern measurements of the non-symbiotic thermocline dwelling species *Ndut* reveals a $\delta^{15}N$ elevation of around 1‰ with respect to the nitrate consumed in the euphotic zone [1,2]. In our data, FB-$\delta^{15}N_{Tsacc}$ (Fig. S2) varies from 5‰ to 7.5‰ and FB-$\delta^{15}N_{Ndut}$ from 6‰ to 8‰, which indicates the $\delta^{15}N$ of the nitrate supply to be between 5‰ to 7.5‰ and an offset between the two species of 0.5-1‰. The sample resolution of *Tsacc* is limited due to sporadic appearance of the species. In the latter half of the study interval, there are several gaps where the average sample resolution differs from the 10-20 cm average and decreases to 60-123 cm. We therefore decided to combine the two species' FB-$\delta^{15}N$ data by calculating the average of their $\delta^{15}N$ (FB-$\delta^{15}N_{NTC}$; Fig. S2c). It is based on the average $\delta^{15}N$ difference of 0.81‰ between the two species at sample depths both species were measured (Fig. S2d). This value was then subtracted from the *Ndut* data to produce assumed *Tsacc* $\delta^{15}N$ values. The combined FB-$\delta^{15}N_{NTC}$ containing the most prominent features of the dataset from Site 662 is therefore used in the main text to represent the thermocline and thus nutricline $\delta^{15}N$ sea-water nitrate value at this site. The N content for the species measured at Site 662 range from 3.21 to 5.01 µmol/mg with an average of 3.88 µmol/mg for *Ndut*, and 3.41 to 5.02 µmol/mg with an average of 4.19 µmol/mg for *Tsacc*, both showing no correlation with FB-δ15N (Fig. S3).

S2. Updated age models for ODP sites 662 and 999

The age models for both sites are based on alignment of benthic foraminifera $\delta^{18}O$ to the $\delta^{18}O$ benthic stack [3]. We produced a new age model for Site 662 using $\delta^{18}O$ values from the benthic stack as age tie points (Fig. S5). The age of $\delta^{15}N$ samples was then linearly interpolated using Python.

S3. Spectral and cross spectral data analysis

$\delta^{15}N$ values were processed using both the ARAND software [4] and Pyleoclim python script [5]. Initially, all analyzed records were resampled and interpolated at a resolution of 4000 to 5000 kyr, depending on their average original sampling resolution. The $\delta^{15}N$ records were then spectrally analyzed using Continuous Wavelet Transform to estimate the change in time series variance and dominances of orbital scale cycles. Cross spectral coherences and phase relationship with other climatic records was also analyzed using both ARAND (Fig. 3 in the main text) and Cross Wavelet Analysis of Pyleoclim python script (Fig. S8).

S4. Continental shelf area percentage calculation using past sea level modelling

To produce a first-order estimate of continental shelf area changes, we apply the global mean sea level curve of Berends et al. [6] to Pliocene topography as reconstructed by Dowsett et al. [7]. This topography, constructed to represent the mid-Piacenzian (~3.0 Ma) and named PRISM4, accounts for dynamic topography and residual glacial isostatic adjustment signals in modern topography due to Pleistocene ice loading. Used as a boundary condition for the Pliocene Model Intercomparison Project Phase 2 (PlioMIP2), the PRISM4 topography represents the current understanding of Pliocene paleogeography. After merging global mean sea level and topography, we calculate the continental shelf area as the region at each time step extending from mean tide level to -150 meters below sea level.

Beyond the correction included in PRISM4, we choose not to account for Pliocene glacial isostatic adjustment in our calculations. We justify this choice in several ways. First, while Pliocene to modern ice models for Antarctica are accessible (e.g., 8), no such models are freely available for the Northern Hemisphere (sensu 6, 9, 10), which hinders production of Glacial Isostatic Adjustment (GIA) models for this period. Second, although GIA exerts a spatially heterogenous influence on continental shelf area in the late Pleistocene (e.g.: 11), this influence was likely more muted at low- to mid-latitudes during the Pliocene due to the smaller size and loading footprint of the Northern Hemisphere ice sheets.
Using the calculated shelf area and the global mean sea-level, we can then calculate the shelf area percentage with respect to the basin size, presented in Fig. 4 in the main text and Fig. S9.

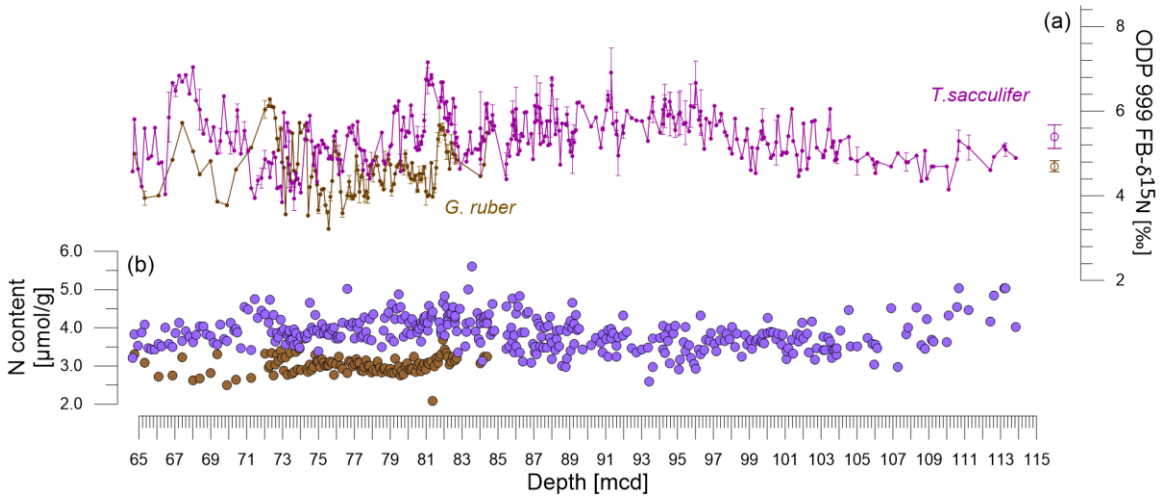

Fig. S1. FB-$\delta^{15}N$ from EEA Site ODP 999 during the PPT. (a) FB-$\delta^{15}N$ measured on the on the euphotic zone dwelling species *T. sacculifer* (purple) and *G. ruber* (brown) (b) N content for both species. The average replicate standard deviation for each species' $\delta^{15}N$ is: *Tsacc* = 0.28 ‰ *Gruber* = 0.13 ‰ (see Data Set S1).

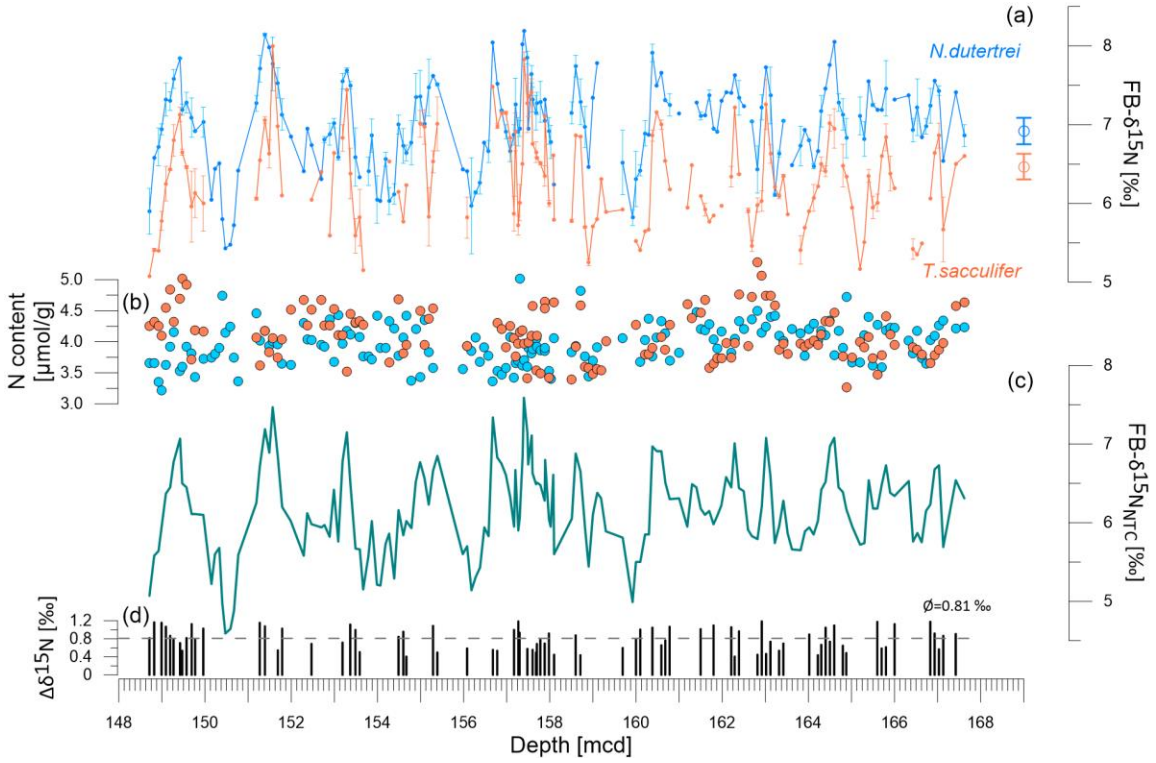

Fig. S2. FB-$\delta^{15}N$ from EEA Site ODP 662 during the PPT. (a) FB-$\delta^{15}N$ measured on the thermocline dwelling species *N.dutertrei* (blue) and on the euphotic zone dwelling species *T.sacculifer* (orange) (b) FB N content for both species. The average replicate standard deviation for each species' $\delta^{15}N$ is: *Ndut* = 0.16 ‰ *Tsacc*=0.17 ‰ (see Data Set S2). (c) Nutricline (NTC) FB-$\delta^{15}N$ (green). (d) Difference FB-$\delta^{15}N_{Ndut}$ - FB-$\delta^{15}N_{Tsacc}$ at depths with measurements for both species, average=0.81‰ (dashed horizontal line) was used for the calculation of the FB- $\delta^{15}N_{NTC}$ (see Supporting Information S1 for more details).

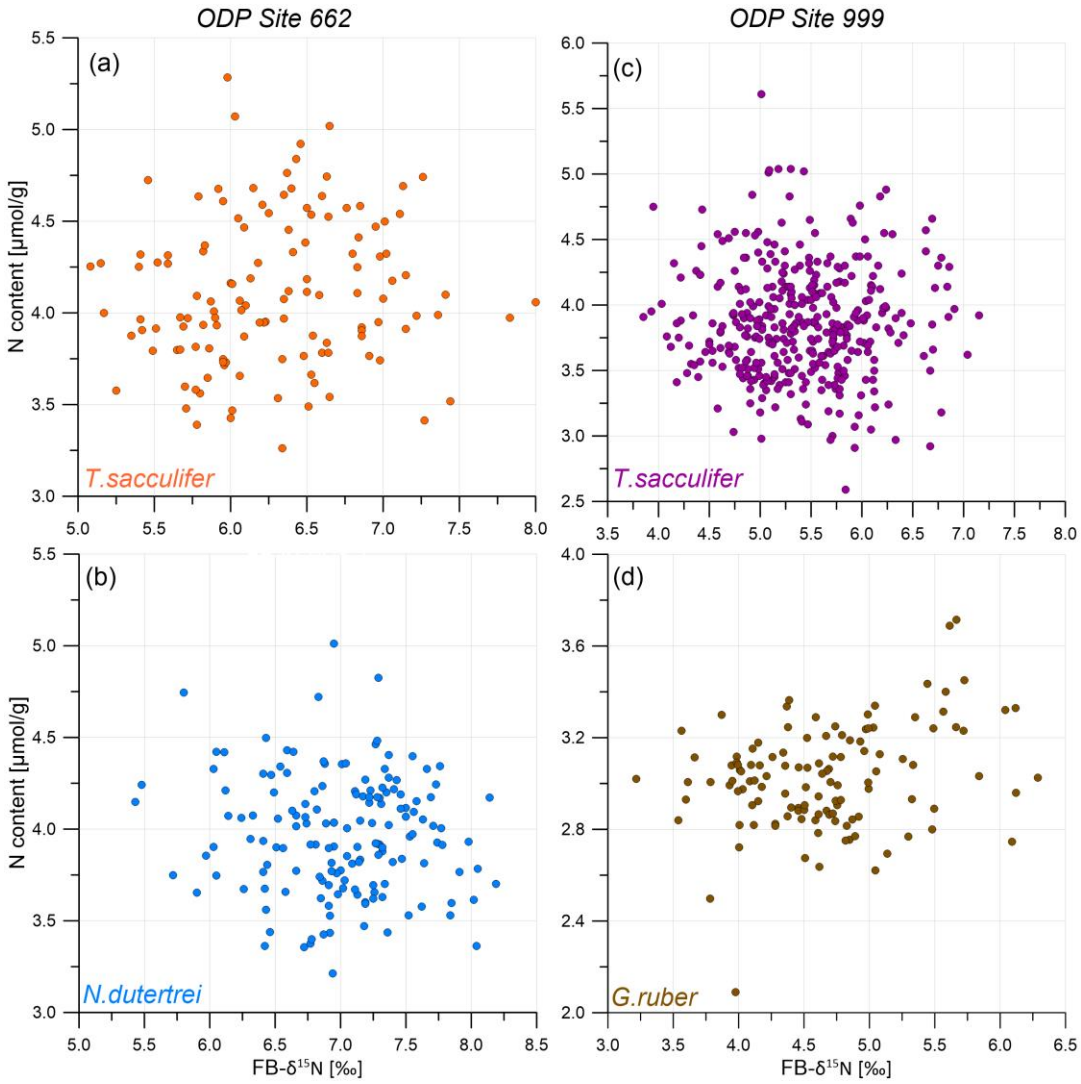

Fig. S3. Cross-plots of N content versus FB-δ^{15}N data from all species measured in the current study. (a) *T.sacculifer* data measured at ODP Site 662**.** (b) *N.dutertrei* data measured at ODP Site 662. (c) *T.sacculifer* data measured at ODP Site 999. (d) *G.ruber* data measured at ODP Site 999. For all species we find no relationship between N content and FB-δ^{15}N.

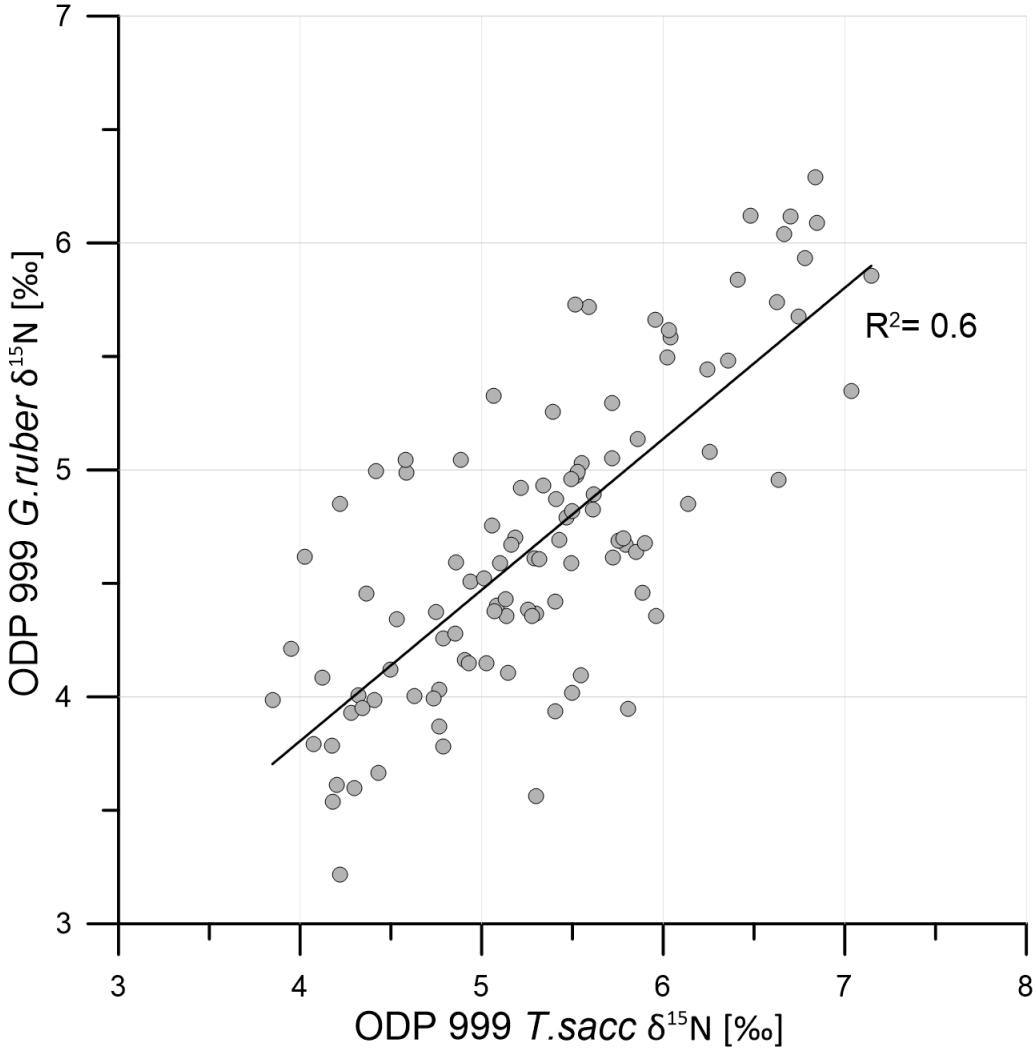

Fig. S4. Comparison of FB-$\delta^{15}N$ data from the two species measured at ODP Site 999, showing a good correlation.

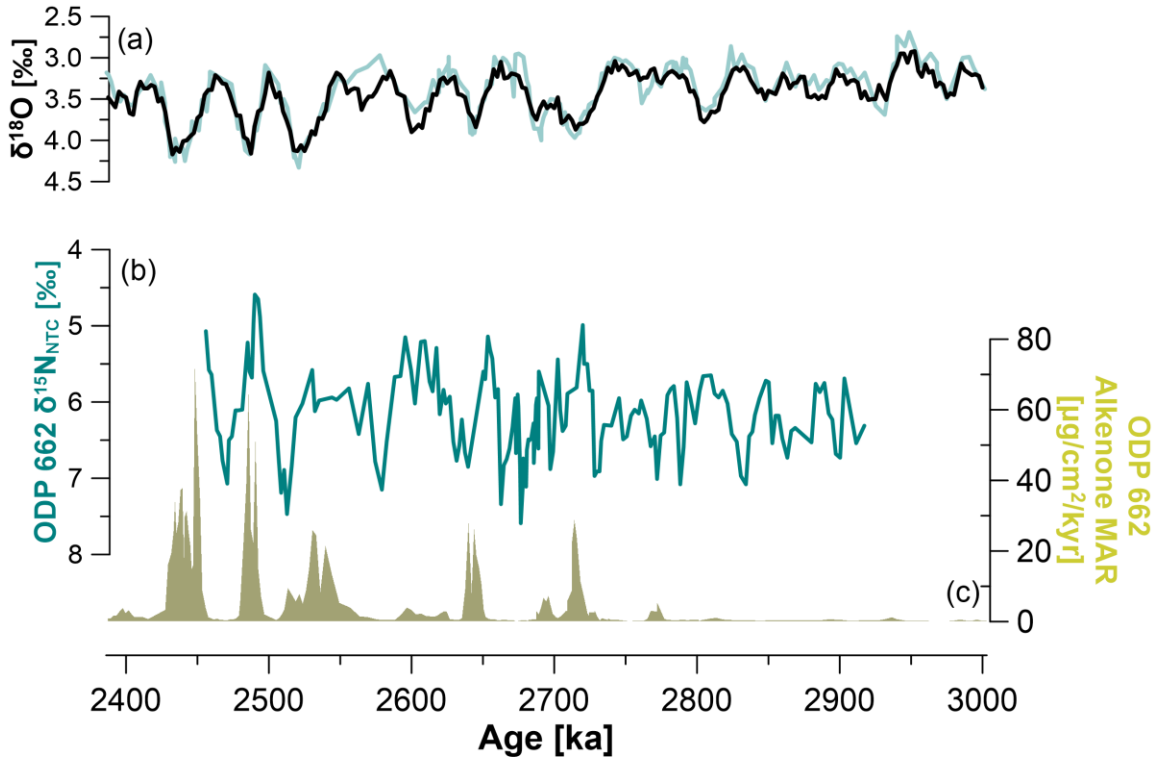

Fig. S5. Orbitally tuned age model for Site 662, FB-$\delta^{15}N$ and alkenone Mass Accumulation Rate (MAR) data. (a) LR04 $\delta^{18}O$ data (black) plotted with ODP 662 (light blue) benthic $\delta^{18}O$ record [3], on which the age model development was based. (b) FB-$\delta^{15}N$ ODP 662 data (teal; this study; 12). (c) ODP 662 alkenone MAR (khaki; 12).

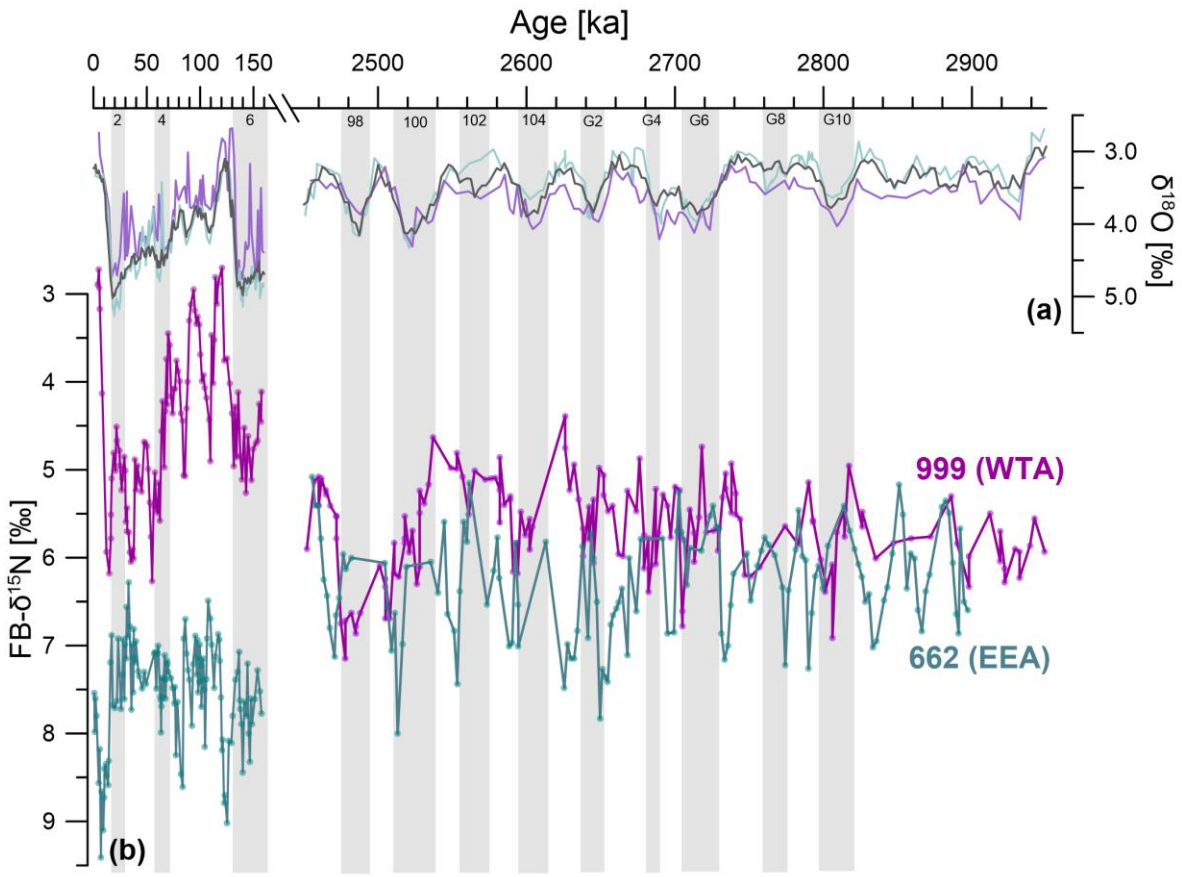

Fig. S6. Zoom-in on FB-δ^{15}N data from ODP Sites 999 in the Western Tropical Atlantic and 662 in the Eastern Equatorial Atlantic, compared to data from the last 160 kyr [11]. (a) δ^{18}O data for Site 999 (light purple) and 662 (light blue) compared to the LR04 benthic δ^{18}O stack (grey; 3). (b) FB-δ^{15}N data from Sites 999 (this study and ref. 13; purple) and 662 (this study and ref. 11; teal). Both records were smoothed using a three-point window to help identify visual features. The vertical grey bands represent Marine Isotope Stages (MIS) since ~2.8 Ma. MIS boundaries were assigned using LR04 information [3].

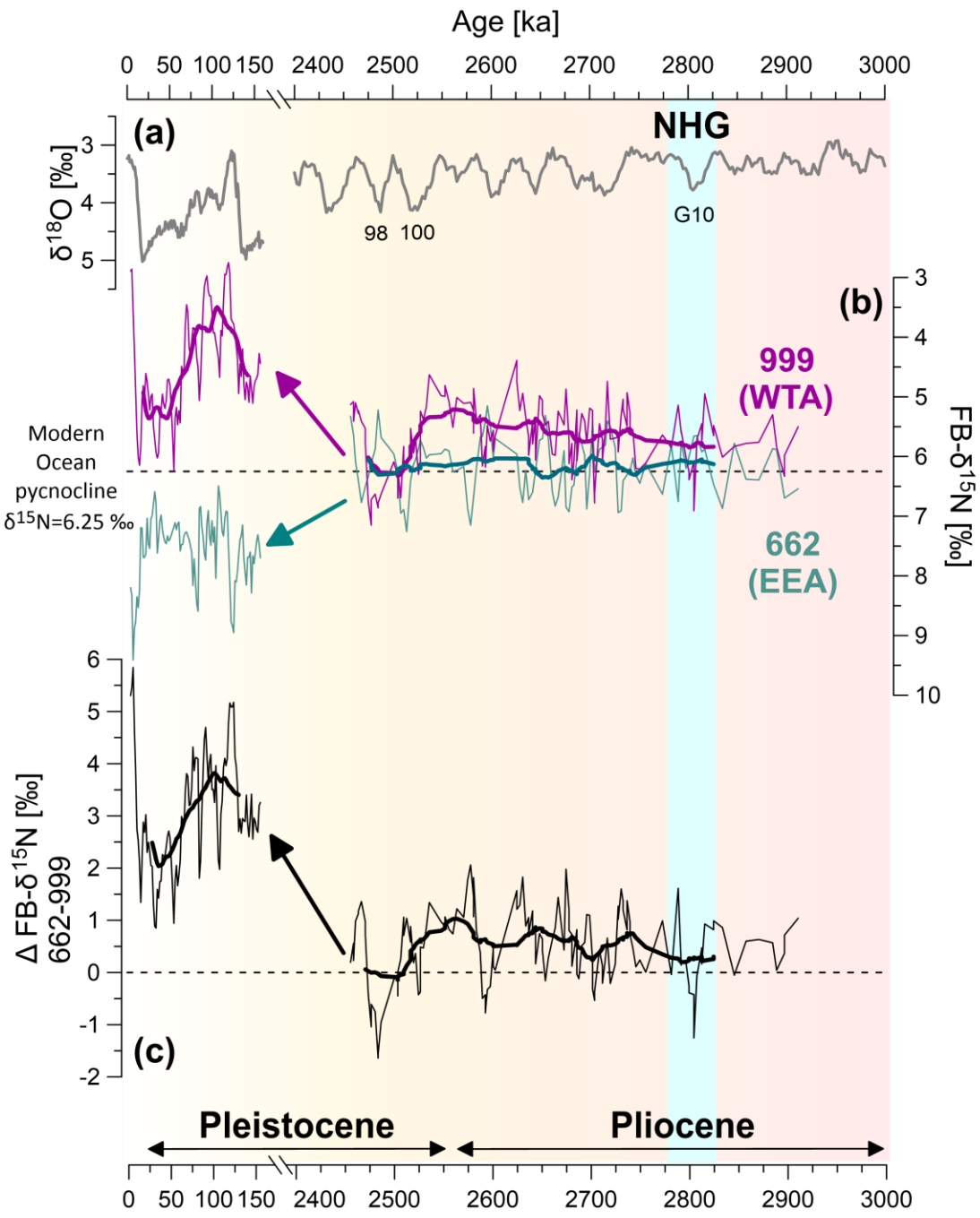

Fig. S7. $\delta^{15}N$ data from ODP Sites 999 in the Western Tropical Atlantic and 662 in the Eastern Equatorial Atlantic, and the difference between them, compared to data from the last 160 kyr [11]. (a) LR04 benthic $\delta^{18}O$ stack (grey; 3). (b) $\delta^{15}N$ data from Sites 999 (this study and ref. 13**;** purple) and 662 (this study and ref. 11; teal). (c) The difference (Δ FB-$\delta^{15}N$= FB-$\delta^{15}N_{662}$ - FB-$\delta^{15}N_{999}$) between $\delta^{15}N$ of the two sites. All records were smoothed over 21-point window to emphasize the long-term trends, showing a smaller difference between the EEA and WTA over the PPT versus the past 160 kyr. The black thick arrow indicates the increase in Δ FB-$\delta^{15}N$ through time. Δ FB-$\delta^{15}N$ was calculated using FB-$\delta^{15}N$ data from Site 662 that was interpolated to match sampling points from Site 999.

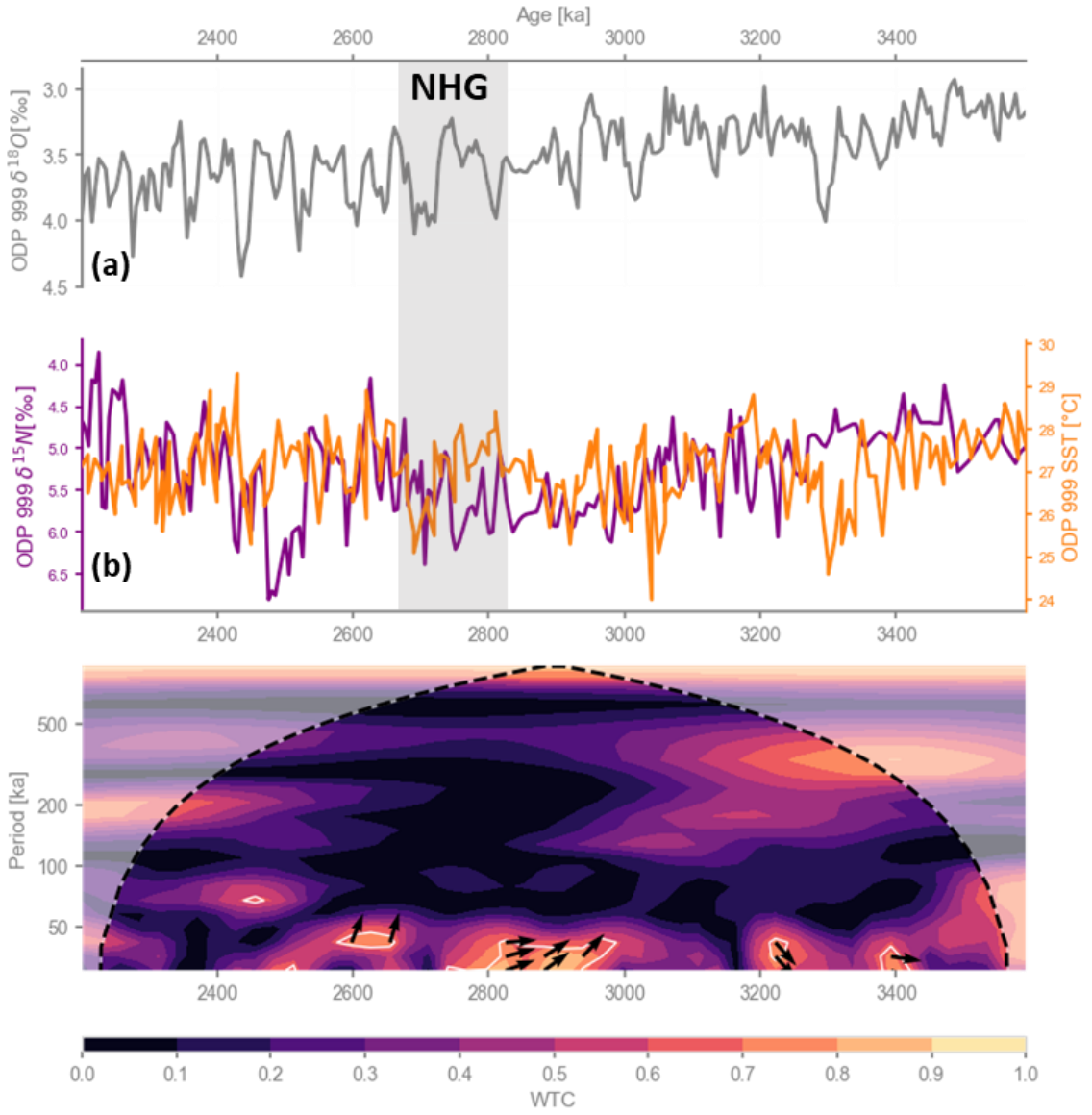

Fig. S8. Wavelet cross coherence (WTC) analysis of PPT $\delta^{15}N$ (this study) and SST records from Site 999 [14]**.** (a) $\delta^{18}O$ record from ODP Site 999 (gray;3). (b) FB-$\delta^{15}N$ record (purple; this study) and SST (orange; 14) from Site 999. (c) Wavelet cross coherence analysis results where a value of 1 is perfect coherence. We find no coherent relationship between FB-$\delta^{15}N$ and SST at ODP Site 999. The white lines delineate regions of the scalogram that are significant against an AR(1) benchmark (AR(1) is a time series model where each value depends linearly on its immediately preceding value plus random noise, capturing short-term memory or persistence in the data), thus encircling “islands” of notable power. Plotting and analysis where conducted using Pyleoclim software [5].

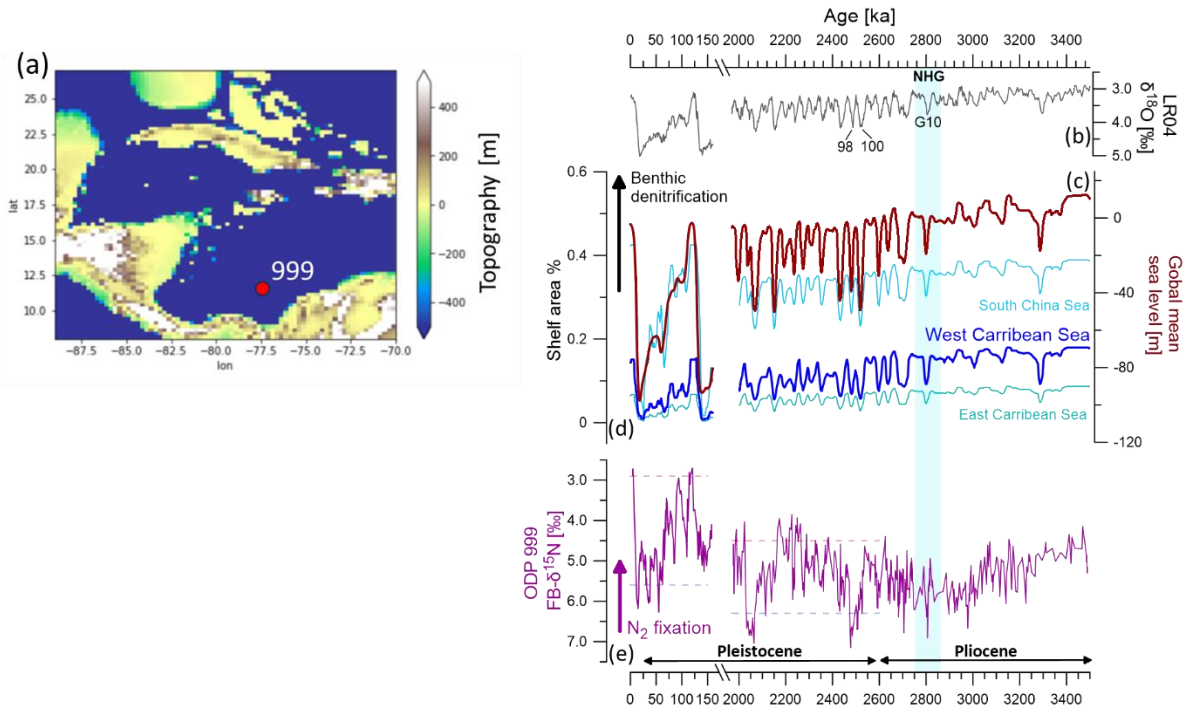

Fig. S9. Comparison of the FB-δ^{15}N data from Site 999 with shelf area percentage changes as a result of sea level fluctuations. (a) Map of the location of ODP Site 999 and the surrounding shelf area (defined as the water depth between 0 and 150 m, see S4 for more details) (b) LR04 benthic δ^{18}O stack [3]. (c) the global mean sea level curve is plotted in dark brown [6] and is compared to (d) changes in shelf area percentage (%) in different basins, where the Western Caribbean Sea area is plotted in dark blue, Eastern Caribbean is plotted in turquois and the South China Sea is plotted in light blue. (e) FB-δ^{15}N from ODP Site 999. The dashed horizontal lines mark the interglacial (orange) and glacial (blue) average FB-δ^{15}N values for the last 160 kyr and the Early Pleistocene respectively. The changes in shelf area percentage are larger during the last 160 kyr in comparison to the PPT. During the PPT, the changes in shelf area percentage are largest in the South China Sea. Shelf area percentage changes are larger in the West Caribbean basin than in the Eastern Caribbean, which could have an effect on the amount of benthic denitrification as suggested in previous studies [15]. Each drop in shelf area percentage corresponds to an increase in FB-δ^{15}N, which is interpreted to represent a reduction in N_2-fixation.

Supplementary Dataset S1 (separate file). ODP Site 999 FB-$\delta^{15}N$.

Supplementary Dataset S2 (separate file). ODP Site 662 FB-$\delta^{15}N$.

Supplementary Dataset S3 (separate file). ODP Site 662 age model LR04 tie points.

SI References

1. Ren, H., Sigman, D. M., Thunell, R. C. & Prokopenko, M. G. Nitrogen isotopic composition of planktonic foraminifera from the modern ocean and recent sediments. *Limnol. Oceanogr.* **57**, 1011–1024 (2012).
2. Smart, S. M. *et al.* Ground-truthing the planktic foraminifer-bound nitrogen isotope paleo-proxy in the Sargasso Sea. *Geochim. Cosmochim. Acta* **235**, 463–482 (2018).
3. Lisiecki, L. E. & Raymo, M. E. A Pliocene-Pleistocene stack of 57 globally distributed benthic d18O records. *Paleoceanography* **20**, 1–17 (2005).
4. Howell, P., Pisias, N., Ballance, J., Baughman, J. & Ochs, L. ARAND Time-Series Analysis Software. at https://github.com/jesstierney/arand (2006).
5. Khider, D. *et al.* Pyleoclim : Paleoclimate Timeseries Analysis and Visualization With Python Paleoceanography and Paleoclimatology. *Paleoceanogr. Paleoclimatologyoge* (2022) doi:10.1029/2022PA004509.
6. Berends, C. J., Boer, B. De & Wal, R. S. W. Van De. Reconstructing the evolution of ice sheets , sea level , and atmospheric CO 2 during the past 3 . 6 million years. *Clim. Past* **17**, 361–377 (2021).
7. Dowsett, H. *et al.* The PRISM4 (mid-Piacenzian) paleoenvironmental reconstruction. *Clim. Past* **12**, 1519–1538 (2016).
8. Pollard, D. & Deconto, R. M. Description of a hybrid ice sheet-shelf model, and application to Antarctica. *Geosci. Model Dev.* **5**, 1273–1295 (2012).
9. Raymo, M. E., Mitrovica, J. X., O'Leary, M. J., DeConto, R. M. & Hearty, P. J. Departures from eustasy in Pliocene sea-level records. *Nat. Geosci.* **4**, 328–332 (2011).
10. Willeit, M., Ganopolski, A., Calov, R. & Brovkin, V. Mid-Pleistocene transition in glacial cycles explained by declining CO2 and regolith removal. *Sci. Adv.* **5**, eaav7337 (2025).
11. Auderset, A. *et al.* Sea Level Modulation of Atlantic Nitrogen Fixation Over Glacial Cycles. *Paleoceanogr. Paleoclimatology* **39**, 1–21 (2024).
12. Lawrence, K. T. *et al.* Time-transgressive North Atlantic productivity changes upon Northern Hemisphere glaciation. *Paleoceanography* **28**, 740–751 (2013).
13. Straub, M. *et al.* Nutrient conditions in the subpolar North Atlantic during the last glacial period reconstructed from foraminifera-bound nitrogen isotopes. **28**, 79–90 (2013).
14. O'Brien, C. L. *et al.* High sea surface temperatures in tropical warm pools during the Pliocene. *Nat. Geosci.* **7**, 606–611 (2014).
15. Ren, H. *et al.* Impact of glacial/interglacial sea level change on the ocean nitrogen cycle. *Proc. Natl. Acad. Sci. U. S. A.* **114**, E6759–E6766 (2017).